



UNIVERSITY OF LEEDS

This is a repository copy of *Solar radiation and functional traits explain the decline of forest primary productivity along a tropical elevation gradient*.

White Rose Research Online URL for this paper:
<http://eprints.whiterose.ac.uk/118230/>

Version: Supplemental Material

Article:

Fyllas, NM, Bentley, LP, Shenkin, A et al. (17 more authors) (2017) Solar radiation and functional traits explain the decline of forest primary productivity along a tropical elevation gradient. *Ecology Letters*, 20 (6). pp. 730-740. ISSN 1461-023X

<https://doi.org/10.1111/ele.12771>

© 2017 John Wiley & Sons Ltd/CNRS. This is the peer reviewed version of the following article: Fyllas, NM, Bentley, LP, Shenkin, A et al. (17 more authors) (2017) Solar radiation and functional traits explain the decline of forest primary productivity along a tropical elevation gradient. *Ecology Letters*, 20 (6). pp. 730-740., which has been published in final form at <https://doi.org/10.1111/ele.12771>. This article may be used for non-commercial purposes in accordance with Wiley Terms and Conditions for Self-Archiving.

Reuse

Items deposited in White Rose Research Online are protected by copyright, with all rights reserved unless indicated otherwise. They may be downloaded and/or printed for private study, or other acts as permitted by national copyright laws. The publisher or other rights holders may allow further reproduction and re-use of the full text version. This is indicated by the licence information on the White Rose Research Online record for the item.

Takedown

If you consider content in White Rose Research Online to be in breach of UK law, please notify us by emailing eprints@whiterose.ac.uk including the URL of the record and the reason for the withdrawal request.



eprints@whiterose.ac.uk
<https://eprints.whiterose.ac.uk/>

Supporting Information

S1. Study Sites and Stand Productivity Estimation

Our study area is located along a 3300 m elevation gradient in the tropical Andes and extends to the Amazon Basin. Across this transect a group of ten intensively monitored 1-ha plots was established as part of the long-term research effort coordinated by the Andes Biodiversity Ecosystems Research Group (ABERG, <http://www.andesconservation.org>) and the ForestPlots (<https://www.forestplots.net/>) and Global Ecosystems Monitoring Network (GEM; <http://gem.tropicalforests.ox.ac.uk/projects/aberg>) networks. In this study we exclude SPD-02, which is located on a landslide prone ridge just below cloud and was always an outlier in our simulations as well as in other studies across the gradient (Malhi et al. 2017a). Table S1.1 provides a summary of the environmental conditions for the study sites. Five of the plots are montane plots in the Kosñipata Valley, spanning an elevation range 1500 - 3500 m (Malhi et al. 2010), two are submontane plots located in the Pantiacolla front range of the Andes (range 600 - 900 m) and two plots are found in the Amazon lowlands in Tambopata National Park (elevation range 200 - 225 m). The elevation gradient is very moist (Table S1.1), with seasonal cloud immersion common above 1500 m elevation (Halladay et al. 2012), and no clear evidence of seasonal or other soil moisture constraints throughout the transect (Zimmermann et al. 2010). Plots were established between 2003 and 2013 in areas that have relatively homogeneous soil substrates and stand structure, as well as minimal evidence of human disturbance (Girardin et al. 2014).

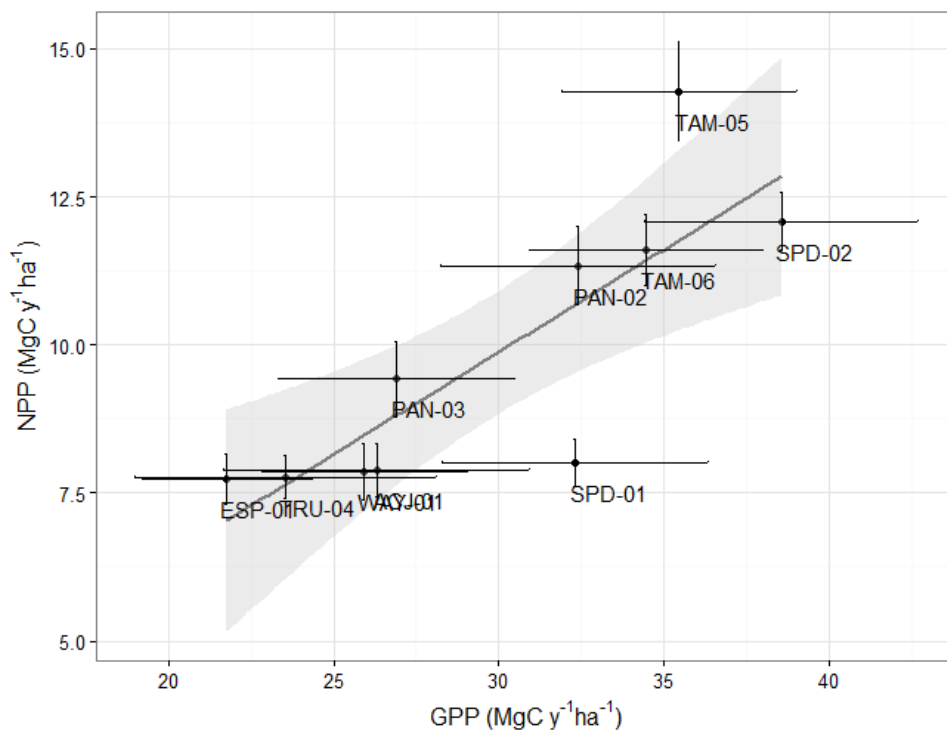
At all plots, the GEM protocol for carbon cycle measurements was employed (www.gem.tropicalforests.ox.ac.uk). The GEM protocol involves measuring and summing all major components of NPP and autotrophic respiration on monthly or seasonal timescales (Malhi et al. 2017a). NPP measurements include: canopy litterfall, leaf loss to herbivory, aboveground woody productivity of all medium-large ($D > 10$ cm) trees (every three months), annual census of wood productivity of small trees (D 2-10 cm), branch turnover on live trees, fine root productivity from ingrowth cores installed and harvested (every three months) and estimation of coarse root productivity from aboveground productivity. Autotrophic respiration (R_a) is calculated by summing up rhizosphere respiration (measured monthly), aboveground woody respiration estimated from stem respiration measurements (monthly) and scaling with surface area, belowground coarse root and bole respiration (fixed multiplier to stem respiration) and leaf dark respiration estimated from measurements of multiple leaves in two seasons. GPP, the carbon assimilated via photosynthesis is approximately equal to the amount of carbon used for NPP and R_a , thus $GPP = NPP + R_a$. Finally the proportion of total GPP invested in NPP, the carbon use efficiency is estimated by $CUE = NPP / GPP$.

For six of the plots, NPP and GPP were estimated by summation of the measured and estimated components of NPP and autotrophic respiration (Malhi et al. 2017a). For the remaining plots, we used measured NPP to estimate GPP applying the mean carbon use efficiency of the other plots, separated into cloud forest and submontane/lowland plots.

Table S1: Environmental characteristics of the study sites. Note that the annual solar radiation, mean temperature and total precipitation values refer only to year 2013.

Site Code	Lat	Lon	Elevation (m asl)	Solar Radiation ($\text{GJ m}^{-2} \text{yr}^{-1}$)	Mean annual Temperature ($^{\circ}\text{C}$)	Annual Precipitation (mm)
TAM-05	-12.83	-69.27	223	4.80	24.6	2078
TAM-06	-12.84	-69.30	215	4.80	24.6	2078
PAN-02	-12.65	-71.26	595	3.82	23.8	3156
PAN-03	-12.64	-71.27	859	3.82	22.0	3156
SPD-01	-13.05	-71.54	1713	4.35	17.2	3694
TRU-04	-13.11	-71.59	2719	3.49	13.0	3570
ESP-01	-13.18	-71.59	2868	3.51	12.3	1796
WAY-01	-13.19	-71.59	3045	3.51	11.1	1796
ACJ-01	-13.15	-71.63	3537	4.23	7.3	2088

Figure S1: Estimated NPP ($\pm 2\text{se}$) versus GPP ($\pm 2\text{se}$) across the Amazon-Andes elevation gradient. The slope of the linear regression indicates the average plot-level CUE.



S2. Model Description

The original TFS model is a trait-continua and individual-based model, which simulates the carbon (C) balance of each tree in a stand (Fyllas et al. 2014). The model is initialised with tree-by-tree diameter at breast height (D) and functional traits data. Four functional traits [leaf dry mass per area (LMA in g m^{-2}), leaf N (N_{Lm} in mg g^{-1}) and P (P_{Lm} in mg g^{-1}) mass-based concentrations and wood density ρ_{w} (g cm^{-3})] are used to represent a continuum of tree functional properties. Rather than grouping trees into plant functional types, TFS implements distributions of functional traits and thus a continuum of plant strategies and responses to environmental conditions can be simulated. Leaf mass per area, wood density and maximum tree height seem to consistently influence competitive interactions across plant species (Kunstler et al. 2016) and can be good candidate traits to represent the global “fast-slow” plant economics spectrum (Reich 2014). In TFS, the three leaf traits (LMA, N_{Lm} , P_{Lm}), the central components of the leaf economic spectrum, regulate the photosynthetic capacity and the respiration rate of trees (Wright et al. 2004, Atkin et al. 2015). Wood density (ρ_{w}) accounts for variation in aboveground biomass (M_{A} in kg DM), with trees of greater ρ_{w} supporting a higher biomass for a given D and tree height (Chave et al. 2014). Allometric equations are used to infer tree height (H in m) and allocation to leaf (M_{L}), stem (M_{S}) and root (M_{R}) biomass (all in in kg DM). Light competition is approximated through the perfect plasticity assumption, with tree H used to estimate the relative position of an individual within the canopy, and thus the available solar radiation (Strigul et al. 2008). The carbon and water balance of each tree is estimated on a daily time-step and at the end of each simulation year, stand-level GPP and NPP is estimated by summing up the daily individual-tree C fluxes.

The version of the model used in this study replaces the original CO_2 assimilation [coupled Farquhar - stomatal conductance model, Fyllas et al. (2014)] and C allocation algorithms with the growth equation of Enquist et al. (2007b). Here we give a detailed description of the model, emphasising on the coupling of the integrative growth equation with the climate and solar radiation components of TFS. In particular the model of Enquist et al. (2007b) does not include any temperature or light availability effects on leaf photosynthetic rates and thus spatial and temporal variation of the thermal and irradiance conditions cannot be specifically modelled. We address these shortcomings by allowing the model to estimate an individual-specific daily growth that is driven by variation in temperature and irradiance (and potentially soil moisture) using the algorithms described in the following paragraphs.

1. Tree Allometry

The diameter at breast height (D in cm) along with the four functional traits of (LMA , N_{Lm} , P_{Lm} and ρ_w) is used to functionally define each tree in a plot. For each study site the model is initialised with measured tree D and trait values. Allometric equations relating tree height (H) and crown area (C_A) were taken from Shenkin et al. (2016, under review). In all cases mixed-effect linear regression models were fit to account for species (fixed) and site (random) effects. The general form of these equations is implemented in TFS. Tree height (in m) is estimated from D (cm):

$$H = \exp(\alpha_H + \beta_H \log_{10}(D)) \quad (1)$$

with $\alpha_H = 1.51$ and $\beta_H = 0.084$

The exponent of the C_A versus D scaling relationship is considered well conserved across tropical tree species (Farrion et al., 2016), and this was also verified from the analysis of our data. Crown area (in m^2) is given from:

$$C_A = \alpha_C D^{\beta_C} \quad (2)$$

with $\alpha_C = 0.695$ and $\beta_C = 1.305$

Aboveground tree biomass (M_A in kg) is estimated from Chave et al. (2014) equation:

$$M_A = \alpha_A \cdot (\rho_w \cdot D^2 H)^{\beta_A} \quad (3)$$

with $\alpha_A = 0.0673$ and $\beta_A = 0.976$ and thus for a given D , trees with greater ρ_w achieve a greater M_A . Leaf (M_L), stem (M_S) and root (M_R) biomass (all in kg) are calculated from aboveground biomass:

$$M_L = \alpha_L M_A^{\beta_L} \quad (4a)$$

$$M_S = \alpha_S M_A^{\beta_S} \quad (4b)$$

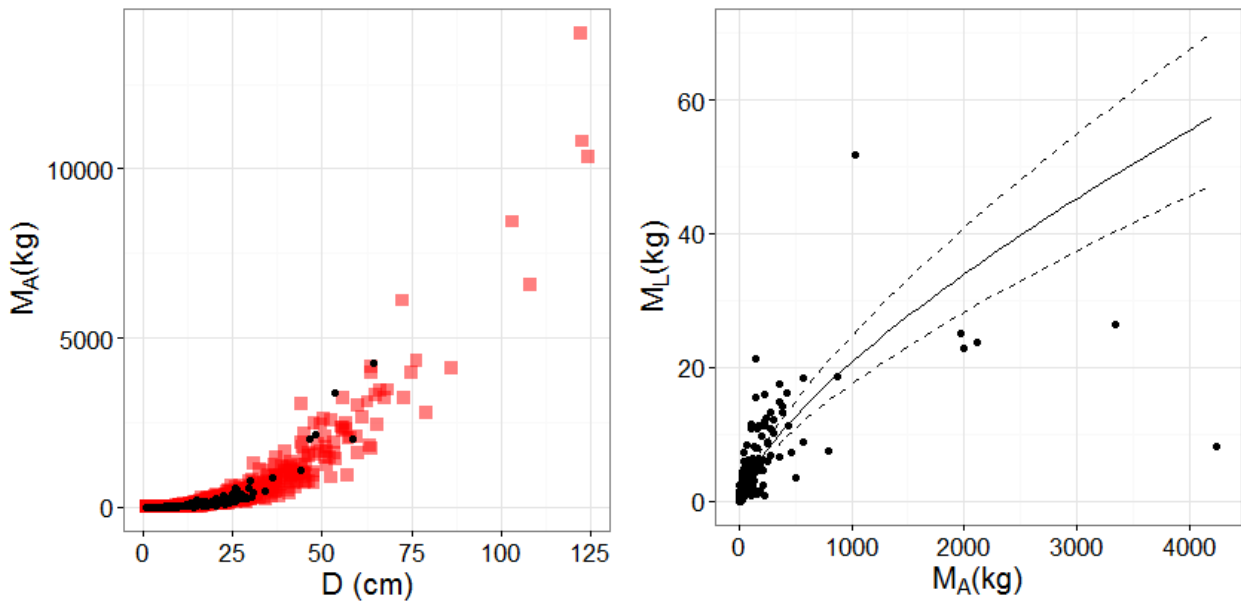
$$M_R = \alpha_R M_A^{\beta_R} \quad (4c)$$

The coefficients of these equations were estimated by fitting standardised major axis (SMA) lines with data from the BAAD dataset (Falster et al. 2015). We only used data from evergreen angiosperms species found in tropical rainforests and tropical seasonal forests with $D > 1$ cm, as within our plots most species are evergreen and only individuals of $D > 2$ cm are included in the productivity calculations. In our simulations, in order to account for potential variation across individual tree architecture we allowed the allometric coefficients to vary within the 95% confidence intervals estimated by the SMAs (Fig S2.1). Total tree biomass is then given from:

$$M_T = M_L + M_S + M_R \quad (5)$$

We note that for the simulations performed in this study the estimation of M_S , M_R and M_T are not required, as the growth rate of trees is expressed only as a function of foliage mass (equation 6). Equation 3 adequately predicted M_A when compared with the records reported in BAAD (Fig S2.1). The range of M_L allometries allowed within our simulations is illustrated in Fig S2.1.

Figure S2.1: Allometric equations used to predict total aboveground biomass (M_A) and total dry leaf biomass (M_L). Left panel: Red squares indicate predictions from the Chave et al. (2014) equation (equation 3) and black circles measurements reported in the BAAD dataset (Falster et al. 2016). The RMSE for predicted and reported M_A was 143 kg. Right panel: The allometric relationship between dry leaf biomass (M_L) and M_A . The black line represents the power function $M_L = \alpha_L M_A^{\beta_L}$ with $\alpha_L=0.158$ and $\beta_L=0.707$, while the broken lines indicate the range of allometries allowed in our simulations within the 95% CI of the SMA estimates [$\alpha_L=(0.150 - 0.166)$ and $\beta_L=(0.690 - 0.724)$].



2. Tree Growth

The relative growth rate (RGR) of a plant (the rate of increase in plant mass per unit of mass present) can be factored to the following three components: the leaf net carbon assimilation rate, the leaf area per unit leaf mass and the leaf weight ratio (Hunt 1982; Lambers et al. 2008). Enquist et al. (2007b) extended this equation to include additional functional traits and the effect of plant size on growth rate:

$$\frac{dM_T}{dt} = \left(\frac{c}{\omega} A_{L,D}\right) \left(\frac{a_L}{m_L}\right) M_L \quad (6)$$

where M_T is the total plant dry biomass (kg), c the carbon use efficiency (no units), ω the fraction of whole-plant dry mass that is carbon, $A_{L,D}$ the leaf area specific photosynthetic rate ($\text{gC cm}^{-2} \text{day}^{-1}$),

a_L the individual leaf area (cm^2), m_L the individual leaf mass (g) and M_L the total leaf dry mass (kg). The time step in our simulations (dt) is daily.

In our simulations a random carbon use efficiency (c) is assigned to each tree in a plot, drawing from a normal distribution $c = (\bar{c}, \sigma)$ with $\bar{c} = 0.33$ and $\sigma = 0.04$, the values estimated from field observations at the plot level, which found no trend in c with elevation (Malhi et al. 2017a). The ω term is set constant to 0.5 ($\text{gC g}^{-1}\text{DM}$). The expression of the photosynthetic rate $A_{L,D}$ is also extended here to account for inter- and intra- specific variability due to leaf traits as well as to light availability (see Photosynthesis section). The α_L/m_L ratio is the inverse of LMA (i.e. SLA) and it is allowed to vary across individual trees.

The basic assumption in equation 6 is that whole-plant net biomass growth rate scales isometrically with total plant leaf biomass (Hunt 1982). However, predicting the patterns of plant biomass allocation is a topic of extensive debate with Metabolic Scaling Theory (MST) suggesting relative invariant power laws (Enquist et al. 2007a) and other studies showing that scaling varies across species and plant sizes (Poorter et al. 2015). Another critique of MST-based growth equations is that they do not take into account resources availability, for example light in forest stands (Muller-Landau et al. 2006, Coomes & Allen 2009). In order to implement equation 6 within TFS and deal with the above critics we 1) used a set of allometric equations with stochastic scaling coefficients estimated from available data and 2) expressed the photosynthetic rate $A_{L,D}$ as a function of both leaf traits (that vary in a continuous way across individual trees) and irradiance that takes into account competition for light between individuals.

As discussed in the previous section (Tree Allometry) the scaling coefficient, β_L , of the $M_L = \alpha_L M_A^{\beta_L}$ relationship is allowed to vary across our simulations within the $(0.690 - 0.724)$ range predicted from the SMA fits of the BAAD dataset. This coefficient is usually denoted as θ in MST studies (Enquist et al. 2007a) and can be considered as an additional “functional trait” that reflects the geometry of the branching network. The exact value of θ has been vigorously debated with recent analyses suggesting that it ranges in a continuous way with ontogeny and decreases from seedlings to mature trees (Poorter et al. 2015). We note however that in our simulations the smallest tree included had an $M_A \approx 3 \times 10^3$ g DM and the biggest one an $M_A \approx 23 \times 10^6$ g DM suggesting that within this range the β_L scaling exponent could vary from ca 0.7 to 0.58 (Poorter et al. 2015), being at a relative stable region. The sensitivity analysis of the model to variation in the β_L parameter can be found in Fig S2.6. This analysis indicates that GPP and NPP simulations are sensitive to the value of β_L value although this should change in combination with the normalization coefficient α_L and not independently as was the case in the sensitivity analysis.

3. Light Competition

One of the key criticisms of MST-based growth equations is that they fail to model asymmetric competition for light (Muller-Landau et al. 2006, Coomes and Allen 2009). In order to account for light competition between trees, we allowed $A_{L,D}$ to vary not only due to the functional properties of a tree's foliage but also based on its relative position within the canopy. Light availability (I) for each individual in the stand is estimated using the built-in canopy structure algorithm of TFS (Fyllas et al. 2014), based on the Perfect Plasticity Approximation (PPA - Purves et al. 2008). In the original TFS model, trees are classified at a canopy or sub-canopy group, with the latter group receiving less radiation. Here we use a more detailed light availability profile, where more than one canopy layers can be identified within a plot (Strigul et al. 2008). A critical height (Z_L^*) is estimated for each layer (L). Trees that are taller than $Z_{L=1}^*$, i.e. canopy trees, receive the full amount of daily radiation. Trees with height between $Z_{L=1}^*$ and $Z_{L=2}^*$, are shaded by the first layer and so on. Each layer is assumed to have a constant leaf area index equal to the ratio of the total stand's LAI with the number of canopy layer identified. Based on its relative position within the canopy (number of shading layers), light availability for each tree is estimate following the Beer's light extinction model with an extinction coefficient $K=0.5$. Our simulations suggest that accounting for asymmetric light competition is important in order to adequately simulate forest productivity along the study gradient (S5 - Light Competition).

Bohlman and Pacala (2012) applied a similar multilayer version of the PPA model in Barro Colorado Island and noted that the understorey layers ($L>1$) are probably not continuous and coherent. Thus in our implementation of the PPA, where layers are considered continuous, their relative importance for shading is probably overestimated in contrast with the underestimation of the first ($L=1$) canopy layer. Both Bohlman and Pacala (2012) and Farrior et al. (2016) used PPA to approximate light competition but implemented species independent growth rates within their simulations. Our approach further enhances their approach, by also considering continuous between-tree variation in potential growth rates emerging from differences in individual-tree functional traits.

4. Photosynthesis

In order to account for inter- and intra- specific variability in the leaf specific photosynthetic rates we used an independent dataset of 136 (one leaf per tree) light response curves and leaf traits measurements in 14 plots along the Amazon-Andes gradient (Atkin et al. 2015; Weerasinghe 2015), and expressed $A_{L,D}$ (equation 6) as a function of the three (LMA , N_{Lm} and P_{Lm}) functional traits. There were six common plots (TAM-5, TAM-06, SPD-01, TRU-04, ESP-01 and WAY-01) with our study

sites, although the elevation range covered (ca 100 to 3450 m asl), includes most of our study sites with the exception of the uppermost plot (ACJ-01, 3537 m asl).

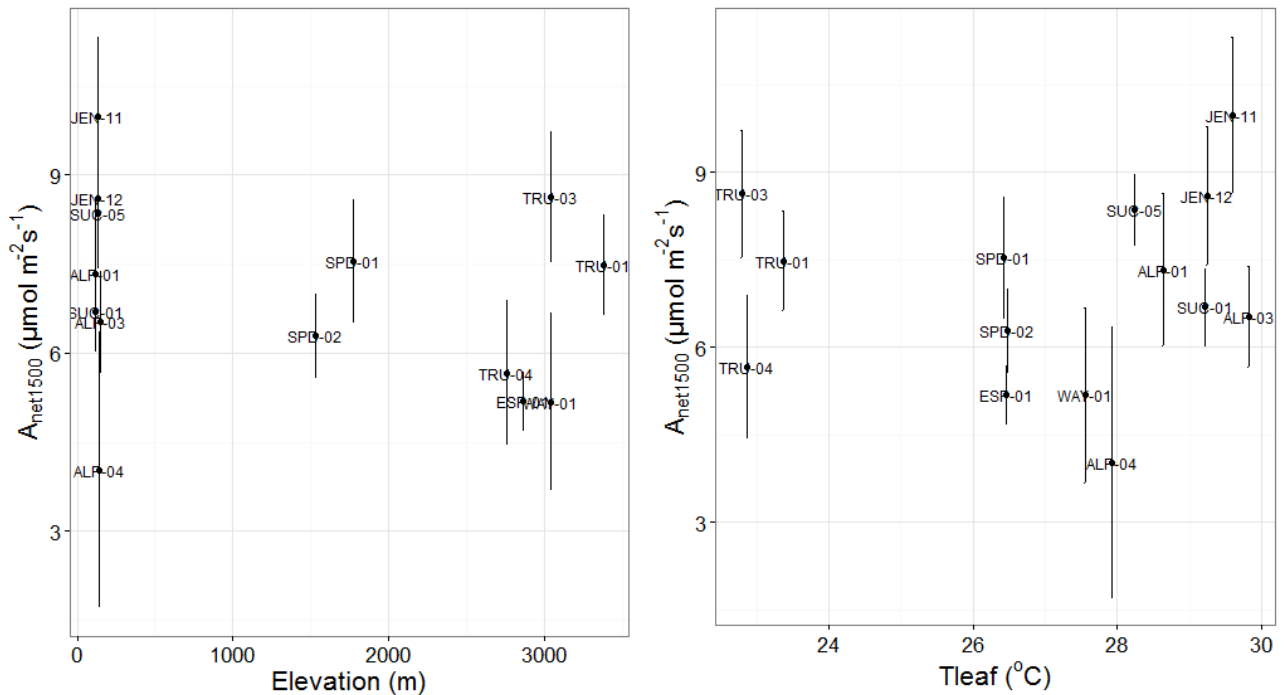
The light-response curve measurements were made using one cut branch per tree, with measurements of net CO₂ exchange (A_{net}) taking place between 10.00 am and 3.00 pm. Measurements were made on the most recently fully expanded leaves attached to the cut branches (which had been re-cut under water immediately after harvesting to preserve xylem water continuity) using the LICOR 6400XT system (LI-COR Inc., Lincoln NE, USA). The block temperature was set to that of the prevailing air temperature at each site at the time of measurements (20°C at the upland sites, and 28°C at the lowland sites). The area-based net photosynthetic rate (A_{net} $\mu\text{mol m}^{-2} \text{s}^{-1}$) was measured starting at 2000 $\mu\text{mol photons m}^{-2} \text{s}^{-1}$ and gradually decreased to darkness via 1500, 1000, 250, 100, 80, 60, 55, 50, 45, 40, 35, 30, 25, 20, 15, 10, 5 and 0 $\mu\text{mol photon m}^{-2} \text{s}^{-1}$ with relative humidity between 60-70% and CO₂ concentration set at 400 ppm. An equilibrium period of two minutes was allowed at each irradiance level before A_{net} was measured.

The plot-level analysis of this dataset (136 leaves/trees) suggest that the area-based net light-saturated photosynthetic rate (at 1500 $\mu\text{mol photons m}^{-2} \text{s}^{-1}$) at the prevailing air temperature ($A_{\text{net}1500}$) did not show any trend with elevation or leaf temperature (Fig S2.2). This is in agreement with the findings of Malhi et al. (2017a), where at ambient temperatures there was no evidence of a trend of photosynthetic parameters with elevation.

A recent study reported that, along the Andean elevation gradient, maximum carboxylation and electron transport rates at a measurement temperature of 25°C were significantly higher at upland sites, possibly reflecting greater P per unit leaf area at high elevations and/or thermal acclimation to sustained lower growth temperatures (Bahar et al. 2016). By contrast, when measurements of gas exchange were made at late morning to early afternoon at each site (20-28°C; Fig S2.2), light-saturated, area-based rates of net photosynthesis, as well as maximum carboxylation and electron transport rates, show no significant trend with elevation (Bahar et al. 2016, Malhi et al. 2017a). The latter observations support the use of a temperature-independent equation for photosynthetic carbon assimilation in our simulations. We note, however, that our photosynthetic light response curves were parameterised with measurements made at leaf temperatures higher than 20°C. For some of the upland sites, leaf temperatures are lower than 20°C for much of the day (van de Weg et al. 2014). This raises the question of whether our estimates of daytime carbon-fixation are an overestimate, given the potential for lower temperatures to reduce net photosynthesis. Currently, there are few data available on how leaf temperatures less than 20°C affect maximum photosynthetic rates along tropical elevation gradients such as that in Peru. A recent study in tropical montane forests in Rwanda showed that while the optimum temperature for photosynthesis of native montane tropical species is lower than that of exotic warm-adapted species, the

temperature range over which optimal rates are exhibited is broad, such that rates at 20°C and 25°C are similar (Varhammar et al. 2015). If the same is true for species adapted to our Andean high elevation plots, then maximum photosynthesis may be relatively temperature insensitive across the dominant daily range of leaf temperatures experienced (i.e. our measurements of leaf photosynthesis would be indicative of carbon uptake rates across a wider range of temperatures experienced by leaves each day at high altitude). Thus although trees in higher elevations operate under lower temperatures, their maximum light-saturated photosynthetic rate is equivalent to their lowland counterparts. The fact that in our dataset $A_{\text{net}1500}$ is higher than would be expected at lower temperatures (upland plots) is because of the higher photosynthetic capacity of the trees found at higher elevations.

Figure S2.2 Plot average net light-saturated (at 1500 $\mu\text{mol photons m}^{-2} \text{s}^{-1}$) photosynthetic rate (\pm standard error) at prevailing air temperature against site elevation and average leaf temperature. No trend was observed in either case (Kendall's $\tau = -0.209$, $p = 0.331$ and $\tau = 0.077$, $p = 0.747$).



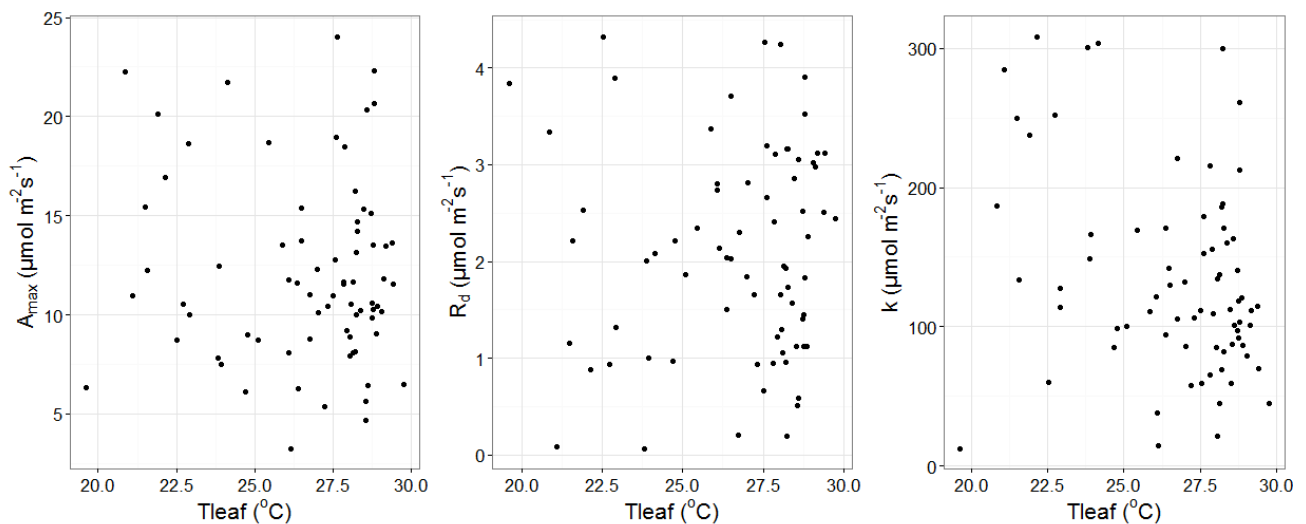
Measurements of the instantaneous net photosynthetic rate (A_{net}) at different light intensities were subsequently used to fit the Michaelis-Menten (MM) light response model for each curve. The MM model was fit by applying the Differential Evolution (DE) algorithm (DEoptim R-package) to minimise the sum of squares. Chen et al. (2016) have shown that the DE provides robust estimates for various photosynthetic light response models and it is not sensitive to initial values selection. The MM light response model is given by the following equation:

$$A_{\text{net}} = \frac{A_{\text{max}} I}{k + I} - R_d \quad (7)$$

where I ($\mu\text{mol m}^{-2}\text{s}^{-1}$) the irradiance, A_{max} the maximum gross photosynthetic rate ($\mu\text{mol m}^{-2}\text{s}^{-1}$), k the half saturation coefficient ($\mu\text{mol m}^{-2}\text{s}^{-1}$) and R_d is the non-photorespiratory mitochondrial CO_2 release taking place in the light (i.e. respiration in the light) ($\mu\text{mol m}^{-2}\text{s}^{-1}$). The low light part ($I < 60 \mu\text{mol m}^{-2}\text{s}^{-1}$) of the curve was excluded in order to minimize the effects of the ‘Kok effect’ (Kok 1948), as the inhibitory effect of light diminishes as irradiance approaches darkness, resulting in increased rates of respiration in darkness compared to those in the light (e.g. Weerasinghe et al. (2014)).

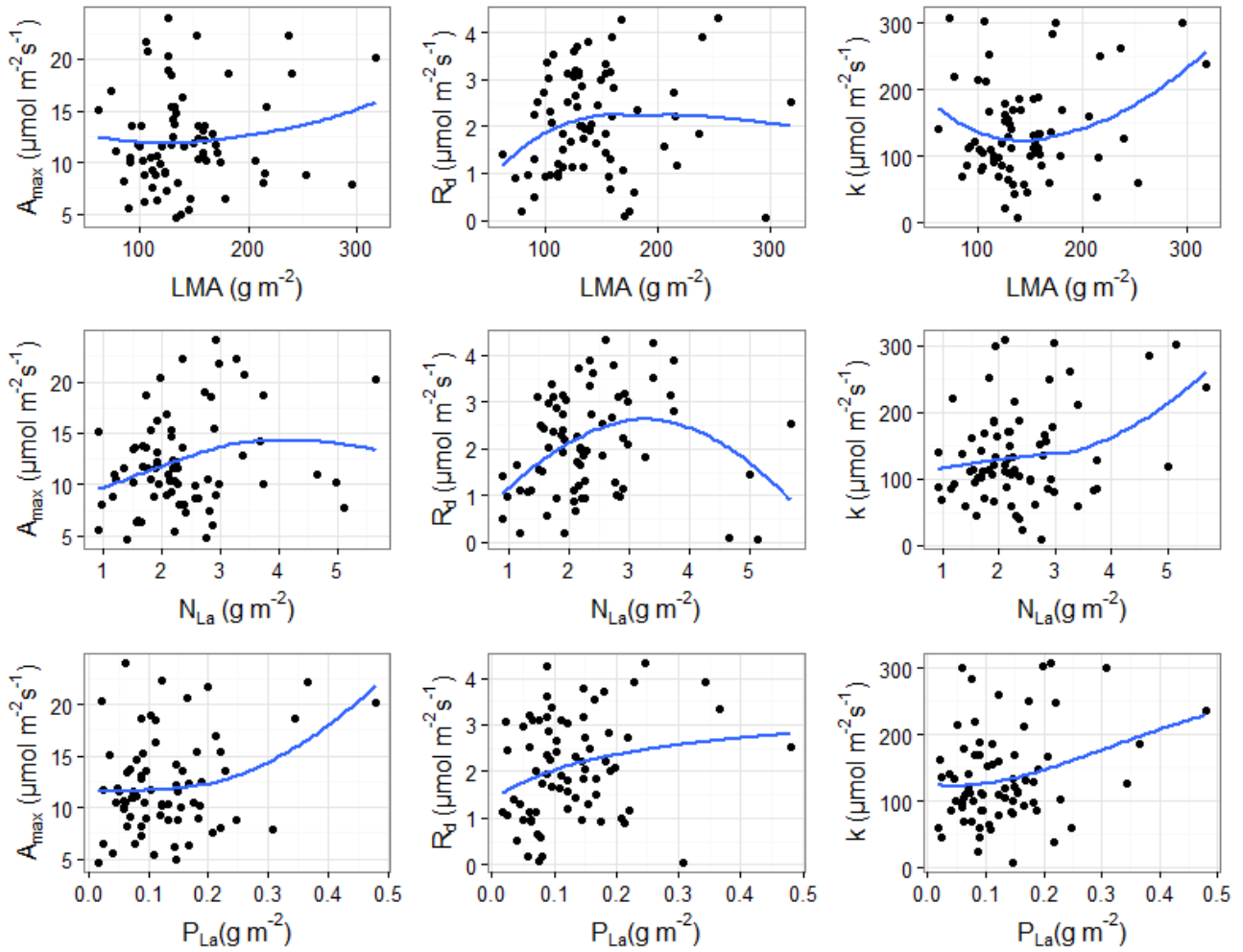
As for some curves the MM parameter estimates were unreasonable, we only used individual curves with estimates of $R_d > 0$ ($\mu\text{mol m}^{-2}\text{s}^{-1}$), $R_d < 4.5$ ($\mu\text{mol m}^{-2}\text{s}^{-1}$) and $k < 400$ ($\mu\text{mol m}^{-2}\text{s}^{-1}$) for further analysis (72 curves). Figure S2.3 illustrates the leaf-specific estimates of MM model for each light response curve versus average leaf temperature. No trend of A_{max} nor R_d was found with leaf temperature, in agreement with the constant A_{net1500} at ambient temperatures. On the other hand, the estimated half saturation coefficient (k) presented a decreasing trend with leaf temperature (Kendall’s $\tau = -0.19$, $p = 0.018$).

Figure S2.3: Leaf-specific estimates of the Michaelis Menten light response curve parameters versus leaf temperature. No trend was identified in A_{max} and R_d with leaf temperature, while k decreased with leaf temperature (Kendall’s $\tau = -0.19$, $p = 0.018$).



We initially explored how the estimated parameters of the MM equation (A_{max} , k , R_d) varied (Fig S2.4) with the three leaf traits, expressed on an area basis (LMA , N_{La} and P_{La}). A_{max} increased with P_{La} supporting the role of leaf P in controlling leaf photosynthesis in tropical forests, R_d increased with LMA and P_{La} with higher P concentration associated with higher ATP and greater physiological activity and respiration and k increased with N_{La} in accordance with protein rich leaves having a higher light compensation point.

Figure S2.4: Variation of the Michaelis-Menten light response curve parameters against individual leaf traits. The blue lines present local polynomial regressions.



We subsequently used a backward stepwise multiple linear regression to express A_{\max} , R_d and k as a function of the three leaf traits with the initial model including second level interactions of LMA with the two leaf nutrient concentrations (N_{La} and P_{La}). The final models (Table S2.1) were selected by the Akaike information criterion (AIC) criterion. A_{\max} was only related to P_{La} with the model explaining only the 5% of the variation, and thus the overall mean 12.13 ($\mu\text{mol m}^{-2} \text{s}^{-1}$) was considered as the common maximum photosynthetic rate for all trees. The half saturation coefficient (k) was mainly related to leaf nutrients, with the linear model accounting for 20% of variation in k (Table S2.1). Finally, R_d was related to all three leaf traits with the linear model accounting for ca 25% of the variation. These equations were used to parameterise the TFS light response model that accounts for the effects of trait variation on the photosynthetic properties of individual leaves.

An average daily photosynthetic rate A_L ($\text{gC m}^{-2} \text{day}^{-1}$) is estimated for each tree with the parameters of the MM model inferred from its trait values and the equations in Table S2.1. The

average daily light availability is used in equation (7), which is converted to photosynthetic photon flux density (PPFD) assuming a 0.48 PAR to solar short-wave radiation ratio and a solar PAR to conversion factor of $4.6 \mu\text{mol J}^{-1}$. Total foliage absorptance was assumed to be 0.75 (Valladares et al. 2002). The total daily photosynthetic rate $A_{L,D}$ (equation 6) is estimated by multiplying average A_L with the day length.

Table S2.1: Summary of the multiple linear regression models for the parameters of the Michaelis-Menten light response function (dependent variables) and the leaf functional traits (predictors).

Parameter	Intercept	LMA (g m^{-2})	N_{La} (g m^{-2})	P_{La} (g m^{-2})	LMA* N_{La}	LMA* P_{La}	R^2
A_{max} ($\mu\text{mol m}^{-2}\text{s}^{-1}$)	10.25 (***)			15.51 (*)			0.056
k ($\mu\text{mol m}^{-2}\text{s}^{-1}$)	162.68 (**)	-0.524	-96.227 (*)	1351.03 (**)	0.753 (**)	-8.216 (**)	0.199
R_d ($\mu\text{mol m}^{-2}\text{s}^{-1}$)	-0.703	0.015 (**)	2.182 (***)	-15.24 (*)	-0.015 (***)	0.131 (***)	0.249

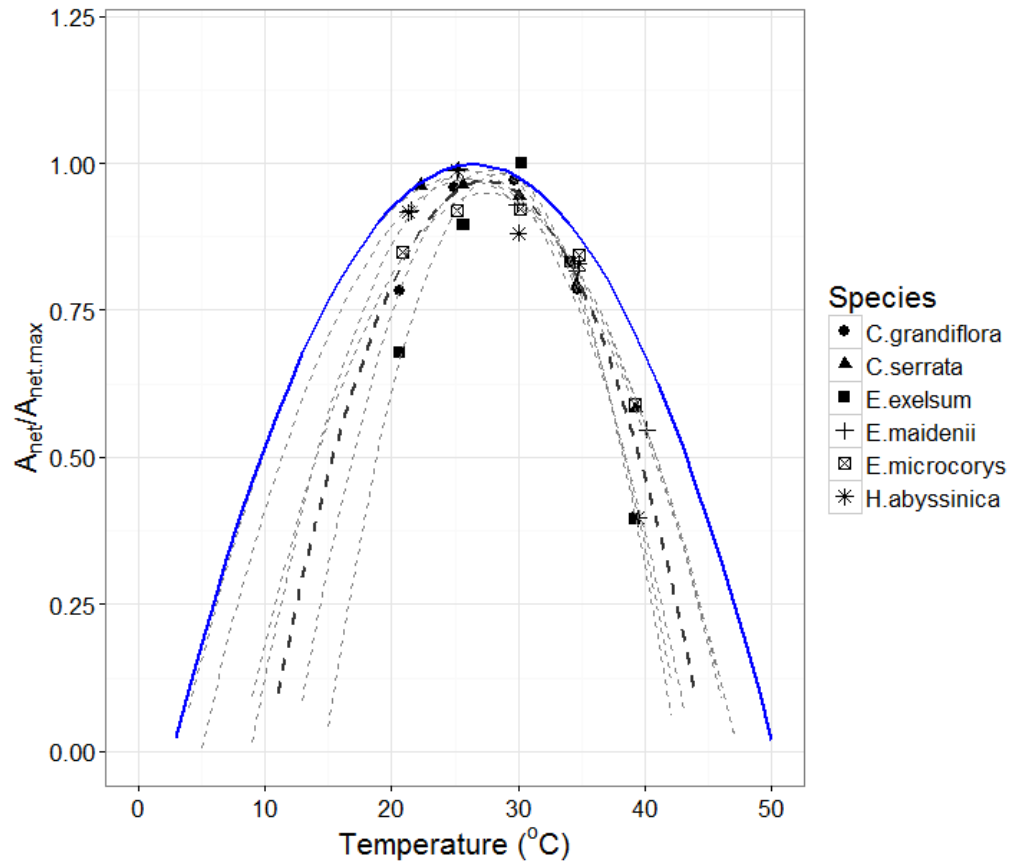
5. Temperature Sensitivity

Although the analysis of the photosynthetic rates data along the elevation gradient support the use of a temperature independent photosynthetic model, we specifically explored whether including a photosynthetic temperature dependence could increase the predictive ability of TFS. For that purpose we employed a normalised temperature response function (Higgins et al. 2016):

$$g(T)=\max(0,-0.242+0.0937T-0.00177T^2) \quad (8)$$

ranging between 0 and 1 and used as a multiplier for A_{net} . The shape of equation 8 was validated against photosynthetic temperature responses data from montane rainforest species in Rwanda (Varhammar et al 2015). A_{net} data of six species at different temperatures were provided (Varhammar pers. comm) and the ratio of A_{net} to the maximum A_{net} measured across the temperature range was estimated. Quadratic curves were fitted for each species and each curve was plotted against the generic model (Fig S2.5). The temperature sensitivity function is used to account for the effects temperature variation on daily photosynthesis. We note that the generic temperature sensitivity model yield a wider curve and thus leads to smaller reductions of A_{net} for given temperature changes compared with the available data. We note that this is the only temperature dependence of the model, as one of our questions was to explore whether explicitly taking into account temperature sensitivity was necessary to model forest productivity along the study gradient.

Fig S2.5. Temperature sensitivity function (blue curve) used in our simulations following the generic model of Higgins et al. (2016). Available data from montane species (broken lines) in Rwanda are also plotted. The thicker broken line represents the average temperature sensitivity across all species.



6. Stand level primary productivity.

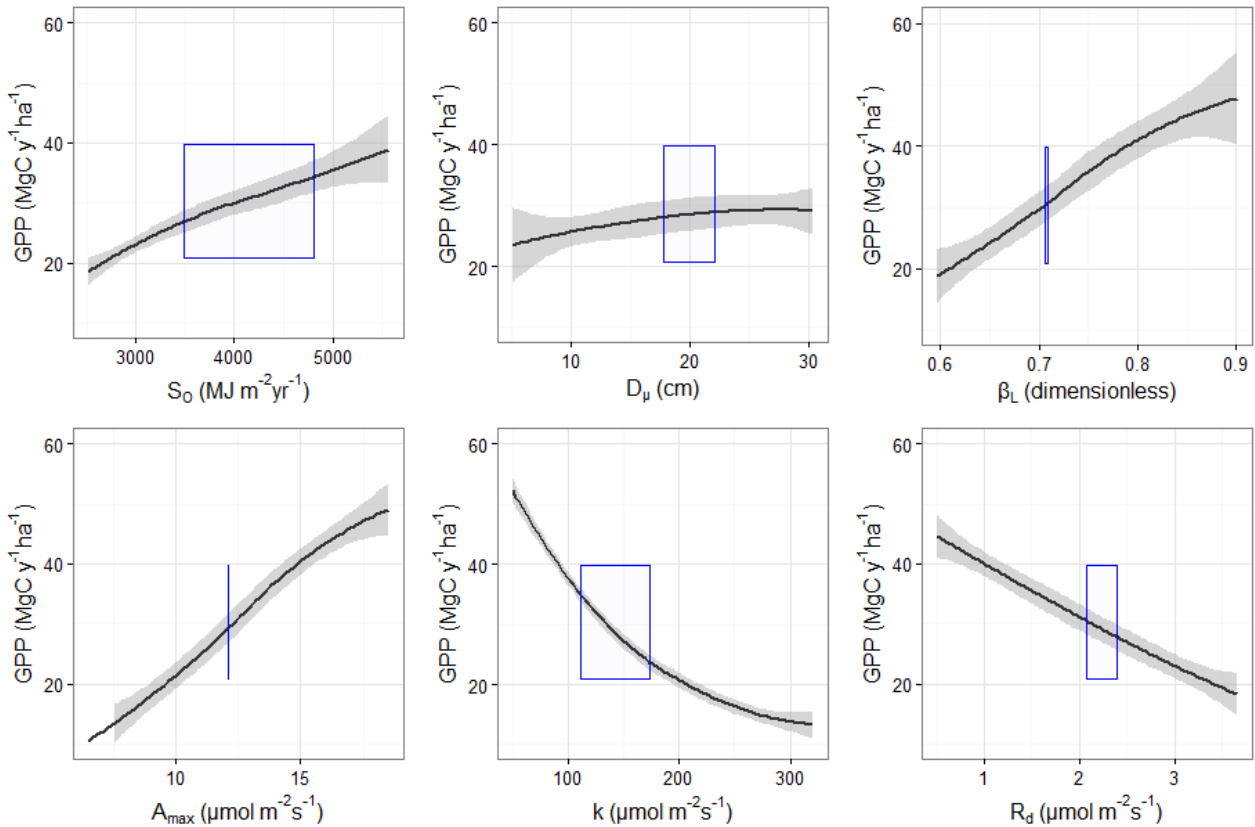
The above equations are applied for each individual within the stand to estimate a daily and at the end of each year an annual growth, i.e. the tree specific NPP. The GPP of each tree is estimated by dividing with the individual specific carbon use efficiency c . The stand level GPP and NPP are estimated by summation of all individual NPPs and GPPs.

7. Sensitivity Analysis

We performed a sensitivity analysis of the simulated GPP by systematically changing the values of a set of key parameters, including the total solar radiation at the top of the canopy S_0 , the mean diameter of the trees (with no change in total stand Basal Area), the value of the β_L (or θ) scaling exponent, as well as the values of the maximum gross photosynthesis (A_{max}), the half saturation coefficient (k) and the respiration (R_d) terms in the light response function. Figure S2.6 summarises

the outputs from the sensitivity analysis. A similar sensitivity of simulated NPP was observed and results are not reported here.

Fig S2.6. Sensitivity analysis of simulated GPP to changes in some key model parameters. The black lines indicate local polynomial regressions of the mean GPP across all plots and the grey area the 95% confidence interval. The area within the blue rectangular shape indicates the range of GPP and the respective model parameter within our simulations.



Simulated GPP was sensitive to changes of radiation S_0 at the top of the canopy with a doubling of S_0 leading to a doubling of GPP. Sensitivity to average stand diameter (D_μ) was explored by maintaining the total stand basal area (BA) and changing the relative size of individual trees. Overall the model was not very sensitive to changes of D_μ suggesting that the relative contribution of different size classes in the total biomass of the stand is not a strong driver of productivity in the model. Simulated GPP was also sensitive to variation of the scaling exponent of the allometric relationship $M_L = \alpha_L M_A^{\beta_L}$, with higher β_L leading to simulations of higher productivity. We note that in the sensitivity analysis we systematically changed β_L without changing α_L . However α_L should co-vary with β_L and thus these simulations are oversensitive to changes in β_L . The model was also sensitive to variation of the parameters of the photosynthetic light response curve, with higher GPP simulated for higher A_{max} and lower GPP simulated for higher k and R_d .

References

1. Atkin, O.K., Bloomfield, K.J., Reich, P.B., Tjoelker, M.G., Asner, G.P., Bonal, D., et al. (2015). Global variability in leaf respiration in relation to climate, plant functional types and leaf traits. *New Phytol*, 206, 614–636
2. Bahar, N.H.A., Ishida, F.Y., Weerasinghe, L.K., Guerrieri, R., O’Sullivan, O.S., Bloomfield, K.J., et al. (2016). Leaf-level photosynthetic capacity in lowland Amazonian and high-elevation Andean tropical moist forests of Peru. *New Phytol*, n/a-n/a
3. Bohlman, S. & Pacala, S. (2012). A forest structure model that determines crown layers and partitions growth and mortality rates for landscape-scale applications of tropical forests. *Journal of Ecology*, 100, 508–518
4. Chave, J., Réjou-Méchain, M., Búrquez, A., Chidumayo, E., Colgan, M.S., Delitti, W.B., et al. (2014). Improved allometric models to estimate the aboveground biomass of tropical trees. *Global change biology*, 20, 3177–3190
5. Chen, L., Li, Z.-B., Hui, C., Cheng, X., Li, B.-L. & Shi, P.-J. (2016). A general method for parameter estimation in light-response models. *Scientific Reports*, 6, 27905
6. Coomes, D.A. & Allen, R.B. (2009). Testing the Metabolic Scaling Theory of tree growth. *Journal of Ecology*, 97, 1369–1373
7. Enquist, B.J., Allen, A.P., Brown, J.H., Gillooly, J.F., Kerkhoff, A.J., Niklas, K.J., et al. (2007a). Biological scaling: Does the exception prove the rule? *Nature*, 445, E9–E10
8. Enquist, B.J., Kerkhoff, A.J., Stark, S.C., Swenson, N.G., McCarthy, M.C. & Price, C.A. (2007b). A general integrative model for scaling plant growth, carbon flux, and functional trait spectra. *Nature*, 449, 218–222
9. Falster, D.S., Duursma, R.A., Ishihara, M.I., Barneche, D.R., FitzJohn, R.G., Vårhammar, A., et al. (2015). BAAD: a Biomass And Allometry Database for woody plants. *Ecology*, 96, 1445–1445
10. Farrior, C.E., Bohlman, S.A., Hubbell, S. & Pacala, S.W. (2016). Dominance of the suppressed: Power-law size structure in tropical forests. *Science*, 351, 155–157
11. Fyllas, N.M., Gloor, E., Mercado, L.M., Sitch, S., Quesada, C.A., Domingues, T.F., et al. (2014). Analysing Amazonian forest productivity using a new individual and trait-based model (TFS v.1). *Geosci. Model Dev.*, 7, 1251–1269
12. Girardin, C.A.J., Espejob, J.E.S., Doughty, C.E., Huasco, W.H., Metcalfe, D.B., Durand-Baca, L., et al. (2014). Productivity and carbon allocation in a tropical montane cloud forest in the Peruvian Andes. *Plant Ecology & Diversity*, 7, 107–123
13. Halladay, K., Malhi, Y. & New, M. (2012). Cloud frequency climatology at the Andes/Amazon transition: 1. Seasonal and diurnal cycles. *J. Geophys. Res.*, 117, D23102
14. Higgins, S.I., Buitenwerf, R. & Moncrieff, G.R. (2016). Defining functional biomes and monitoring their change globally. *Glob Change Biol*, 22, 3583–3593
15. Hunt, R. (1982). Plant growth curves. The functional approach to plant growth analysis. *Plant growth curves. The functional approach to plant growth analysis.*
16. Kok, B. (1948). A critical consideration of the quantum yield of *Chlorella*-photosynthesis. *W. Junk*
17. Kunstler, G., Falster, D., Coomes, D.A., Hui, F., Kooyman, R.M., Laughlin, D.C., et al. (2016). Plant functional traits have globally consistent effects on competition. *Nature*, 529, 204–207

- 18.Lambers, H., Chapin, F.S. & Pons, T.L. (2008). *Plant Physiological Ecology*. Springer New York, New York, NY
- 19.Malhi, Y., Girardin, C.A.J., Goldsmith, G.R., Doughty, C.E., Salinas, N., Metcalfe, D.B., et al. (2016). The variation of productivity and its allocation along a tropical elevation gradient: a whole carbon budget perspective. *New Phytol*, n/a-n/a
- 20.Malhi, Y., Silman, M., Salinas, N., Bush, M., Meir, P. & Saatchi, S. (2010). Introduction: Elevation gradients in the tropics: laboratories for ecosystem ecology and global change research. *Global Change Biology*, 16, 3171–3175
- 21.Muller-Landau, H.C., Condit, R.S., Chave, J., Thomas, S.C., Bohlman, S.A., Bunyavejchewin, S., et al. (2006). Testing metabolic ecology theory for allometric scaling of tree size, growth and mortality in tropical forests. *Ecology Letters*, 9, 575–588
- 22.Poorter, H., Jagodzinski, A.M., Ruiz-Peinado, R., Kuyah, S., Luo, Y., Oleksyn, J., et al. (2015). How does biomass distribution change with size and differ among species? An analysis for 1200 plant species from five continents. *New Phytol.*, 208, 736–749
- 23.Purves, D.W., Lichstein, J.W., Strigul, N. & Pacala, S.W. (2008). Predicting and understanding forest dynamics using a simple tractable model. *PNAS*, 105, 17018–17022
- 24.Reich, P.B. (2014). The world-wide “fast–slow” plant economics spectrum: a traits manifesto. *J Ecol*, 102, 275–301
- 25.Strigul, N., Pristinski, D., Purves, D., Dushoff, J. & Pacala, S. (2008). Scaling from trees to forests: tractable macroscopic equations for forest dynamics. *Ecological Monographs*, 78, 523–545
- 26.Valladares, F., Skillman, J.B. & Pearcy, R.W. (2002). Convergence in light capture efficiencies among tropical forest understory plants with contrasting crown architectures: a case of morphological compensation. *Am. J. Bot.*, 89, 1275–1284
- 27.Vårhammar, A., Wallin, G., McLean, C.M., Dusenge, M.E., Medlyn, B.E., Hasper, T.B., et al. (2015). Photosynthetic temperature responses of tree species in Rwanda: evidence of pronounced negative effects of high temperature in montane rainforest climax species. *New Phytol*, 206, 1000–1012
- 28.Weerasinghe, L.K., Creek, D., Crous, K.Y., Xiang, S., Liddell, M.J., Turnbull, M.H., et al. (2014). Canopy position affects the relationships between leaf respiration and associated traits in a tropical rainforest in Far North Queensland. *Tree Physiol*, 34, 564–584
29. Weerasinghe, K.W.L.K. 2015. Leaf respiration in tropical forests along a phosphorus and elevation gradient in the Amazon and Andes; Leaf respiration in tropical and temperate rainforest tree species: responses to environmental gradients - [PhD] dissertation - Australian National University.
- 30.Weg, M.J. van de, Meir, P., Williams, M., Girardin, C., Malhi, Y., Silva-Espejo, J., et al. (2014). Gross Primary Productivity of a High Elevation Tropical Montane Cloud Forest. *Ecosystems*, 17, 751–764
- 31.Wright, I.J., Reich, P.B., Westoby, M., Ackerly, D.D., Baruch, Z., Bongers, F., et al. (2004). The worldwide leaf economics spectrum. *Nature*, 428, 821–827
- 32.Zimmermann, M., Meir, P., Bird, M.I., Malhi, Y. & Ccahuana, A.J.Q. (2010). Temporal variation and climate dependence of soil respiration and its components along a 3000 m altitudinal tropical forest gradient. *Global Biogeochem. Cycles*, 24, GB4012

S3. Randomisation Exercises

In order to explore the importance of climate, stand structure and functional traits in determining the patterns of forest GPP and NPP across our study sites, we applied within TFS a set of randomization exercises (Table S3.1). To test the importance of climate (Climate only Setup - CoS), we simulated GPP and NPP by using the local (plot-specific) climate and a regional average stand structure and trait distribution (i.e. the average stand structure and traits distribution across all plots along the transect). In order to find a general way to initialise stand structure, we fit the distribution of D with data from all plots to four theoretical distributions including the normal, the lognormal, the Weibull and the Gamma, using the `fitdistrplus` package. From those four distributions, the lognormal was the most appropriate one as it adequately described variation in D across all plots with the lowest AIC (S4). In the CoS, an average regional (i.e. along-transect) stand structure was thus assigned to each plot using the properties of the fitted lognormal distribution (μ and σ). Individual trees were sequentially added in a plot (with D sampled from the regional log-normal distribution) until stand basal area (BA) was $31.4 \text{ m}^2 \text{ ha}^{-1}$, the median BA measured across all plots. The importance of local functional diversity was factored out by initializing trees in the CoS using the average traits distribution across all plots, i.e. using transect-wide instead of local traits distributions. The hypothesis behind the CoS is that climate, and particularly variation in incoming radiation is sufficient to explain variation in productivity across the elevation gradient, with no between-plots variation in traits or stand structure required.

The role of stand structure was tested using the Structure only Setup (SoS). Following this setup, the observed D distribution in each plot was used to initialise trees, with climate and functional diversity showing no variation between plots. In particular, climate was set to be identical across all plots, being assigned the observed climate of one of the mid elevation sites (SPD-01 at 1500 m). The effect of local functional diversity was factored out in a similar way to the CoS, by using a transect-wide traits dataset. The hypothesis behind the SoS is that change in stand structure is the most important determinant of productivity along the elevation gradient. It should be noted that stand structure here mainly expresses the D distribution and not the established biomass, as in TFS the biomass of a tree is also determined by its wood density. Thus this hypothesis does not directly test for the effects of stand biomass on forest productivity but rather for those of the stand's size distribution.

The potential control of functional trait variation, expressed through the distributions of the four traits, was explored by initializing TFS with the locally observed trait distribution and assigning climate and stand-size distribution to fixed values (as above). In the Traits only Setup (ToS), climate was assumed to be common between all plots and assigned the values at SPD-01. Stand structure

was similarly to the CoS initialised for each plot by sampling from the common lognormal distribution until a stand's BA reached the transect-wide median value. Trait values were assigned to each tree in the stand using the built-in trait distribution generator of TFS, which is based on the random-vector generation algorithm of Taylor and Thompson (1986). This algorithm is appropriate for generating non-repeated pseudo-observations from a relatively small sample of observations with approximately the same moments as the original sample. Our hypothesis investigated by this setup is that knowledge of the local distribution of the four functional traits and only a generic description of stand structure and climate is adequate to predict observed variation in GPP and NPP with elevation.

Finally, in the Fully constrained Set-up (FcS), we adopted the plot-specific set-ups of climate, structure and traits (as outlines in the partial set-ups above) as our complete model.

Table S3.1: Summary of the different model setups used in this study. The Fully Constrained setup provides the most data demanding parameterisation where local scale climatic, functional diversity (traits) and stand structure data are required to predict GPP and NPP. The Climate Only setup requires knowledge of local climate and a regional description of trait diversity and stand structure, suggesting that climate is the most important predictor of GPP and NPP. The Structure Only setup requires a detailed description of each stand's structure and regional level climate and traits data, suggesting that stand structure is the most important predictor of GPP and NPP. The Traits Only setup requires a detailed description of each plot's functional traits distributions and regional level data of climate and stand structure, suggesting that functional diversity is the most important predictor of GPP and NPP.

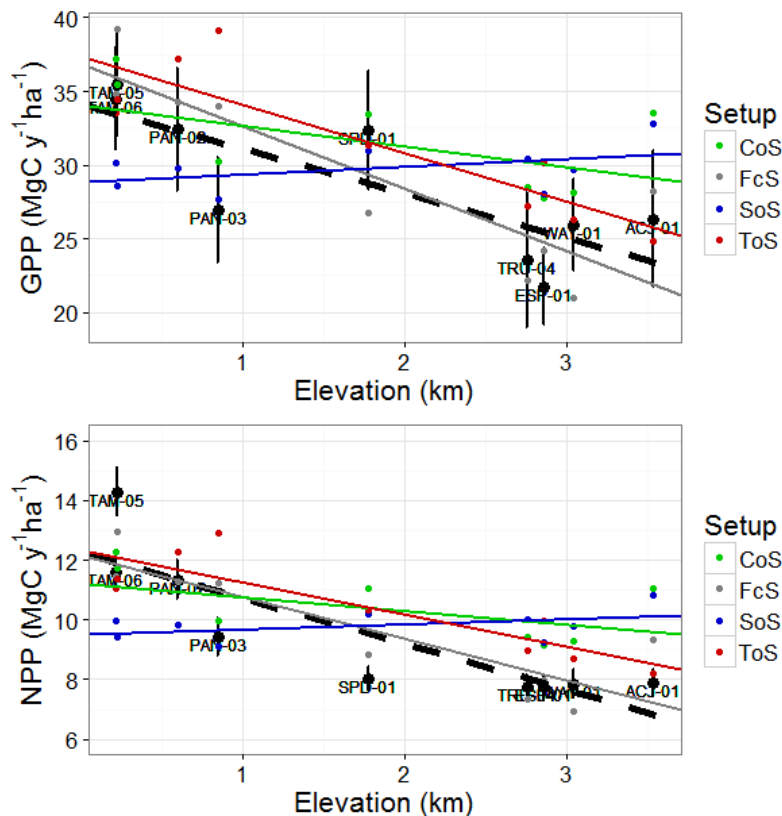
Setup	Climate	Stand Structure	Trait Pool
Fully Constrained FcS	Local	Local	Local
Climate Only CoS	Local	Regional	Regional
Structure Only SoS	Regional Montane	Local	Regional
Traits Only ToS	Regional Montane	Regional	Local

The predictive ability of the various model setups were quantified through standardised major axis (SMA) regressions and estimation of root mean square error (RMSE in $\text{Mg C ha}^{-1} \text{y}^{-1}$) between observed and simulated GPP and NPP (see main text). In addition ordinary least square regressions of simulated GPP and NPP with elevation were performed with the estimated slope (β_{OLS} in $\text{MgC ha}^{-1} \text{y}^{-1} \text{km}^{-1}$) representing the sensitivity of each setup to changes in elevation. Here we present in a greater detail the results of the OLS regressions analyses (Table 3.2, Fig 3.1).

Table 3.2: Parameter estimates of the linear regression of observed and simulated GPP and NPP with elevation. Different model setups are used to explore the productivity sensitivity to climate, stand structure and functional traits. The sensitivity of GPP and NPP to elevation is summarised by the slope linear regression β_{OLS} ($\text{Mg C ha}^{-1} \text{y}^{-1} \text{km}^{-1}$).

Setup	a_{OLS}	std error	β_{OLS}	std error
GPP				
Observations	34.16	1.80	-3.05	0.83
FcS	36.86	1.93	-4.24	0.90
CoS	34.02	1.79	-1.40	0.83
SoS	28.87	0.88	0.51	0.41
ToS	37.32	1.48	-3.26	0.69
NPP				
Observations	12.24	0.75	-1.53	0.35
FcS	12.17	0.64	-1.40	0.30
CoS	11.23	0.59	-0.46	0.27
SoS	9.53	0.29	0.17	0.13
ToS	12.32	0.49	-1.08	0.23

Figure 3.1: Linear regressions of simulated GPP (upper panel) and NPP (lower panel) with elevation. Black points indicate GPP and NPP estimates from observations ± 2 standard errors. The broken black line represents the linear regression of observations with elevation. Grey points are simulations using the fully constrained model (FcS). Green points are simulations using the local climate (CoS) with an average regional structure and trait tree initialisation, blue points are simulations using the local stand structure (SoS) with a regional climate and trait initialisation and red points are simulations using the local traits distributions (ToS) with and average regional climate and structure initialisation. Lines indicate the respective linear regressions, with parameters estimates reported in Table 3.2.



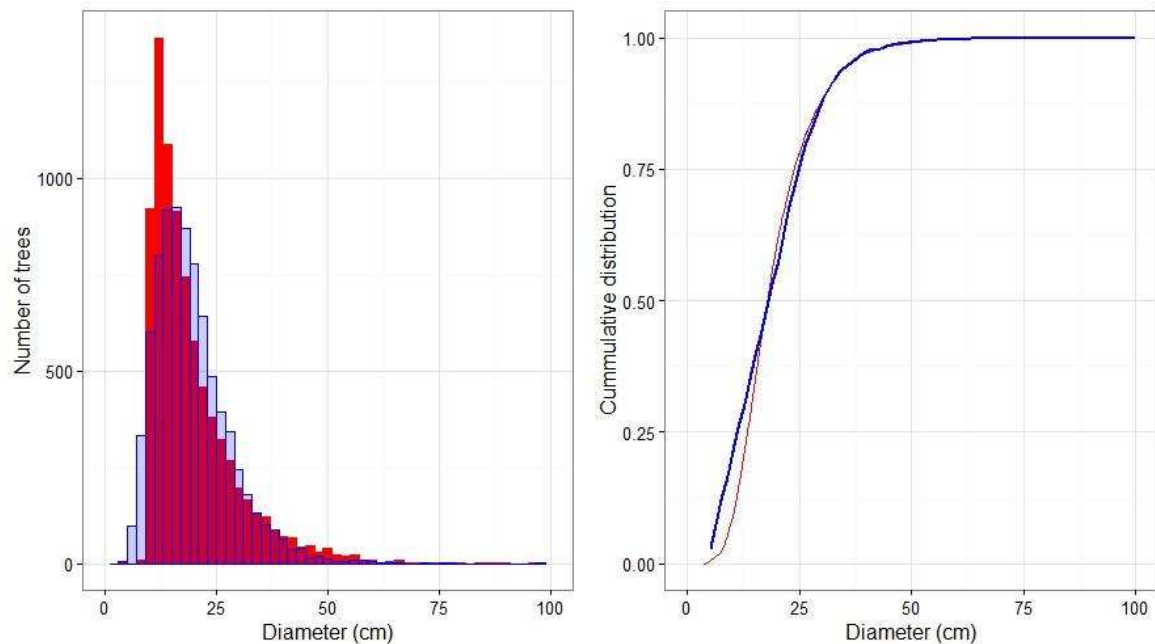
S4. Tree size (D) distribution

Four theoretical distributions were used to describe the diameter at breast height (D) distribution in all study plots. These distributions included the normal the log-normal, the Weibull and the Gamma. We used the fitdistrplus R package to fit individual-tree D measurements to each theoretical distribution and identify which of the four better described the observations. A summary of these fits is provided in Table S4.1. The log-normal distribution better described the observations and thus was used for initialising the model with an average stand structure (Fig S4.1).

Table S4.1: Parameters estimates (\pm standard error) of the four theoretical distributions fitted to individual-tree diameter measurements. The log-normal distribution provided the best fit, achieving the lowest AIC.

Theoretical Distribution	Shape	Scale or Rate	AIC
Normal	19.686 (± 0.116)	10.470 (± 0.082)	61594
Log-normal	2.879 (± 0.005)	0.424 (± 0.003)	56245
Weibull	1.998 (± 0.012)	22.288 (± 0.131)	59453
Gamma	5.128 (± 0.077)	0.261 (± 0.004)	57436

Figure S4.1: Empirical (red) and theoretical (blue) distribution of tree diameter (D) across the Andes-Amazon elevation gradient (left panel). Average stand structure was approximate through the log-normal distribution for D with $\mu=2.879$ and $\sigma=0.424$. The right panel summarises the empirical (red) and theoretical (blue) cumulative distribution functions.



S5. Additional Simulation Exercises

A set of simulation exercises were applied, to explore the importance of temperature, light and functional trait variation within our modelling framework. Below we describe these simulation exercises and summarise some key findings.

Temperature Sensitivity

The importance of the effect of photosynthetic temperature sensitivity was explored following a “leave-one-out” procedure that explored the ability of the model to simulate GPP and NPP patterns under three different model setups: 1) including both photosynthetic temperature sensitivity and functional traits shifts along the gradient, 2) including only temperature sensitivity and 3) including only functional trait shifts. In the first setup simulations were performed with both the temperature sensitivity function (equation 8) and the plot-specific trait initialisation enabled. Thus the effects of temperature on photosynthesis and the effects of environmental conditions (including temperature) on species distribution and associated functional traits shifts along the gradient were taken into account. In the second setup the temperature sensitivity function was enabled but a gradient-wide trait distribution was used, by-passing the effects of functional traits shift along the gradient. In the third case, the photosynthetic temperature sensitivity function was disabled and only the local trait distributions were used, accounting only for the effect of trait shifts.

The outputs of those simulations are summarised in Fig 2 and Table S5.1. Simulations including photosynthetic temperature sensitivity and functional trait shifts along the gradient were too sensitive to elevation changes, underestimating both GPP and NPP particularly at upland sites [GPP: RMSE=9.75, $\beta_{OLS}=-8.90$, NPP: RMSE=2.86, $\beta_{OLS}=-2.94$] (Fig 2, Table SX). A similar model behavior was observed even when only temperature sensitivity was included, assuming no functional traits shift with elevation. However when trait values were allowed to vary with elevation in accordance with observations and temperature sensitivity was excluded, the model illustrated the best model performance [GPP: RMSE=3.25, $\beta_{OLS}=-4.24$, NPP: RMSE=0.99, $\beta_{OLS}=-1.40$]. We defined this model setup, initialized with plot-specific solar radiation, stand structure and functional traits data, as the fully constrained model setup (FcS). The FcS captures the broad gradient between higher productivity in lowland sites and lower productivity in montane sites, suggesting that direct temperature sensitivity could be excluded from our modelling framework (although it could still matter through its effects on traits), and that across the gradient incoming radiation is the main climatic driver of spatial variation in forest productivity.

Table S5.1: Results of TFS performance under different setups. Bold values of the Pearson’s correlation coefficient (ρ) between field measurements and simulations indicate a statistical significant associations ($p < 0.05$). In cases of statistical significant associations a SMA regression was fit and the slope β_{SMA} along with a 95% CI is reported. An adequate model performance is considered when β_{SMA} estimates include 1. RMSE ($\text{Mg C ha}^{-1} \text{ y}^{-1}$) between observations and simulations are also reported with lower values indicating a better model performance. The slope of an ordinary least square regression of simulated productivity with elevation β_{OLS} is also reported here to summarize the sensitivity of GPP and NPP with elevation. For comparison the estimated slope from observations for GPP is -3.05 ($\text{Mg C ha}^{-1} \text{ y}^{-1} \text{ km}^{-1}$) and for NPP is -1.53 ($\text{Mg C ha}^{-1} \text{ y}^{-1} \text{ km}^{-1}$).

Setup	ρ simulations- observations	slope simulations- observations (β_{SMA})	RMSE simulations- observations	slope simulations -elevation (β_{OLS})
GPP				
Temp + Traits	0.82	0.89 (0.68 – 1.16)	9.75	-8.90 (± 0.78)
Temp	0.90	0.84 (0.69 – 1.01)	7.88	-6.61 (± 0.98)
Traits (FcS)	0.77	1.03 (0.93-1.14)	3.87	-4.24 (± 0.90)
NPP				
Temp + Traits	0.86	0.87 (0.70 – 1.09)	2.86	-2.94 (± 0.26)
Temp	0.78	0.82 (0.68 – 1.00)	2.74	-2.18 (± 0.32)
Traits (FcS)	0.90	1.01 (0.93-1.10)	0.99	-1.40 (± 0.30)

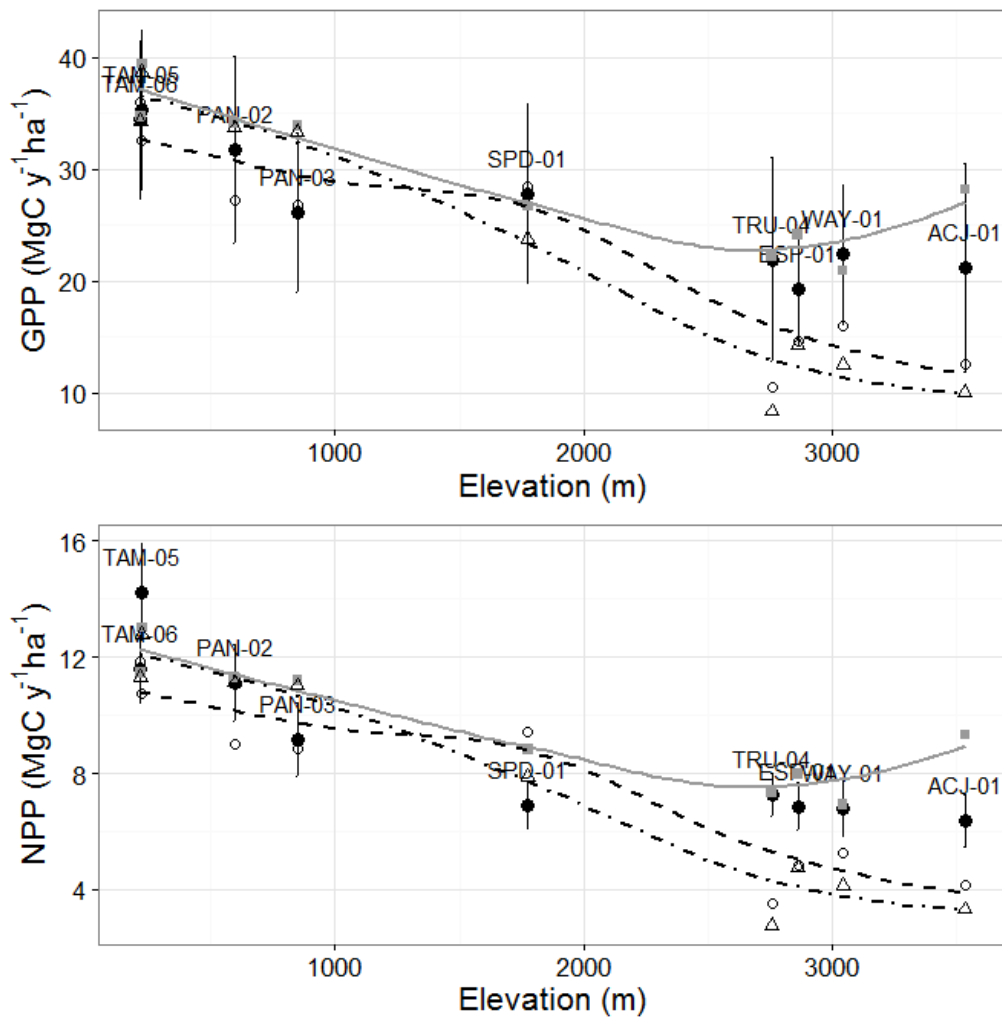
The simulations used to explore for the importance of including a direct photosynthetic temperature dependence were also tested against the ground-area corrected (rather than planimetric) estimates of GPP and NPP (Fig S5.1a). Similar to Table S5.1 the best model performance was observed when the photosynthetic temperature dependence was excluded and variation in functional traits between plots was explicitly taken into account.

Table S5.1a: Results of TFS performance under different setups. Caption identical to Table S5.1 with observed GPP and NPP corrected for the slope of the plots, by dividing planimetric GPP and NPP with the cosine of the slope.

Setup	ρ simulations- observations	slope simulations- observations (β_{SMA})	RMSE simulations- observations	slope simulations -elevation (β_{OLS})
GPP				
Temp + Traits	0.90	0.95 (0.76– 1.18)	7.56	-8.90 (± 0.78)

Temp	0.93	0.89 (0.77 – 1.05)	5.75	-6.61 (±0.98)
Traits (FcS)	0.85	1.10 (1.00-1.20)	4.21	-4.24 (±0.90)
NPP				
Temp + Traits	0.87	0.92 (0.76 – 1.11)	2.29	-2.94 (±0.26)
Temp	0.78	0.86 (0.72 – 1.04)	2.32	-2.18 (±0.32)
Traits (FcS)	0.90	1.07 (0.95-1.20)	1.47	-1.40 (±0.30)

Figure S5.1a: Observed and simulated GPP (upper panel) and NPP (lower panel) along the Andes-Amazon transect. Plot-specific values of climate, forest structure and traits distributions are employed. Black circles are observations (± 2 standard error). Grey squares indicate simulation with no temperature dependence of photosynthesis but with functional traits shift along the gradient. Triangles indicate simulations with temperature dependence of photosynthesis and functional traits shift along the gradient. Open circles indicate simulations including temperature sensitivity but no functional traits shift along the gradient. Lines present local polynomial regressions (loess) of simulated GPP and NPP with elevation under the different model setups. The measured GPP and NPP values are ground-area (rather than planimetric) corrected.



Light Competition

To account for the importance of light competition, we compared the fully constrained model simulations (FcS) that estimates individual-specific light availability with a model setup where light competition was not explicitly simulated and all trees were assumed to receive the full amount of available radiation. The overall model performance significantly decreased when light competition was not taken into account, with the model substantially overestimating both GPP and NPP (Fig S5.2 & Table S5.2). The above suggests that taking into account between-tree variation in light availability is particularly important in order to capture variation in GPP and NPP along the tropical forest elevation gradient.

Figure S5.2: Simulated GPP (upper panel) and NPP (lower panel) using the FcS setup (black squares and black line) which accounts for between trees light competition and the FcS setup that ignores light competition (green squares and green line). Circles indicate field estimates of stand GPP and NPP.

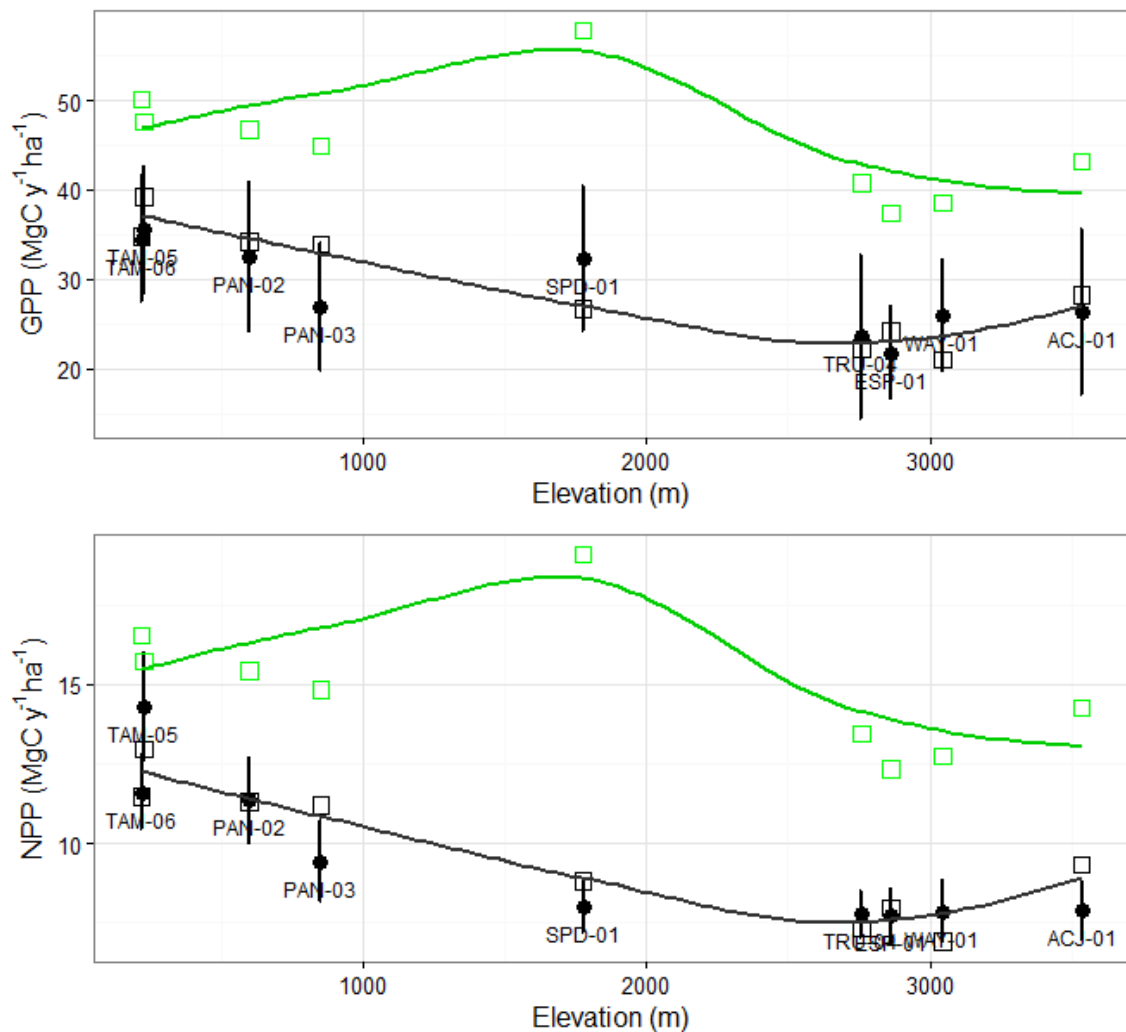


Table S5.2: Comparison of model performance with and without light competition. Bold values of the Pearson’s correlation coefficient (ρ) between field measurements and simulations indicate a statistical significant associations ($p < 0.05$). In cases of statistical significant associations a SMA regression was fit and the slope β_{SMA} along with a 95% CI is reported. An adequate model performance is considered when β_{SMA} estimates include 1. RMSE ($\text{Mg C ha}^{-1} \text{ y}^{-1}$) between observations and simulations are also reported with lower values indicating a better model performance. The slope of an ordinary least square regression of simulated productivity with elevation β_{OLS} is also reported here to summarize the sensitivity of GPP and NPP with elevation. For comparison the estimated slope from observations for GPP is -3.05 ($\text{Mg C ha}^{-1} \text{ y}^{-1} \text{ km}^{-1}$) and for NPP is -1.53 ($\text{Mg C ha}^{-1} \text{ y}^{-1} \text{ km}^{-1}$).

Setup	ρ simulations- observations	slope simulations- observations (β_{SMA})	RMSE simulations- observations	slope simulations -elevation (β_{OLS})
GPP				
FcS - Light	0.77	1.03 (0.93-1.14)	3.87	-4.24 (± 0.90)
FcS -No Light	0.78	1.56 (1.44-1.70)	16.44	-2.71 (± 1.49)
NPP				
FcS - Light	0.90	1.01 (0.93-1.10)	0.99	-1.40 (± 0.30)
FcS -No Light	0.35		5.38	-0.89 (± 0.49)

Importance of elevation shifts in functional traits

In order to explore the effects of functional diversity along the tropical forest elevation gradient two additional simulation exercises were performed, and compared with the FcS model setup. In the first case individuals across all plots were set to have the same functional traits values, i.e. the overall average $LMA=113.8$ (g m^{-2}), $N_{Lm}=21.00$ mg g^{-1} , $P_{Lm}=1.42$ (mg g^{-1}) and $\rho_w=0.57$ (g cm^{-3}). This parameterisation is equivalent to having a single tropical tree PFT across the whole gradient, and thus no species and/or traits turnover with elevation. In the second case, the plot average trait values were assigned to all trees within a plot. This parameterisation is equivalent to have a plot specific PFT and thus partially takes into account functional traits differences between plots associated to species turnover with elevation. However within plot functional variation is not taken into account.

The model performance statistics for these two exercises are compared with the FcS setup in table S5.3 and Fig S5.3. Using a single PFT, i.e. overall average traits values substantially decreased the predictive ability of the model. Furthermore, the decline of GPP and NPP with elevation (β_{OLS}) was not reproduced highlighting the role of functional traits shifts to drive the patterns of forest productivity along the Amazon-Andes gradient. By increasing the number of PFTs and taking into

account species and functional traits turnover with elevation a much better model performance was achieved underlining the importance of species turnover for forest productivity along the study gradient.

Table S5.3: Comparison of model performance with various level of functional diversity representation. Bold values of the Pearson’s correlation coefficient (ρ) between field measurements and simulations indicate a statistical significant associations ($p < 0.05$). In cases of statistical significant associations a SMA regression was fit and the slope β_{SMA} along with a 95% CI is reported. An adequate model performance is considered when β_{SMA} estimates include 1. RMSE ($\text{Mg C ha}^{-1} \text{ y}^{-1}$) between observations and simulations are also reported with lower values indicating a better model performance. The slope of an ordinary least square regression of simulated productivity with elevation β_{OLS} is also reported here to summarize the sensitivity of GPP and NPP with elevation. For comparison the estimated slope from observations for GPP is -3.05 ($\text{Mg C ha}^{-1} \text{ y}^{-1} \text{ km}^{-1}$) and for NPP is -1.53 ($\text{Mg C ha}^{-1} \text{ y}^{-1} \text{ km}^{-1}$).

Setup	ρ simulations- observations	slope simulations- observations (β_{SMA})	RMSE simulations- observations	slope simulations -elevation (β_{OLS})
GPP				
FcS Between and within plot functional trait variation	0.77	1.03 (0.93-1.14)	3.87	-4.24 (± 0.90)
FcS – one PFT No functional trait variation	0.69	0.92 (0.83-1.02)	4.08	-0.72 (± 0.93)
FcS – nine PFTs Between plots functional trait variation	0.85	1.00 (0.91 – 1.10)	3.55	-4.79 (± 0.80)
NPP				
FcS Between and within plot functional trait variation	0.90	1.01 (0.93-1.10)	0.99	-1.40 (± 0.30)
FcS – one PFT No functional trait variation	0.41	0.90 (0.76-1.07)	2.16	-0.24 (± 0.31)
FcS – nine PFTs Between plots functional trait variation	0.89	0.98 (0.90-1.07)	1.02	-1.58 (± 0.26)

Figure S5.3: Simulated GPP (upper panel) and NPP (lower panel) using the FcS setup which accounts for within stand functional trait variation (black symbols and line) with the one PFT setup (blue symbols and line) that does not account for plot-level differences in plant functional traits and the nine PFTs setup (red symbols and line) that accounts for plot-level differences (but not within plot variation) in plant functional traits. Circles indicate field estimates of stand GPP and NPP.

